

Daniel Johansen

# Efficiency improvement of Reversible Pump Turbine operation due to implementation of a booster pump

Master's thesis in Fluid Mechanics

Supervisor: Pål-Tore Selbo Storli

June 2021



Daniel Johansen

# **Efficiency improvement of Reversible Pump Turbine operation due to implementation of a booster pump**

Master's thesis in Fluid Mechanics  
Supervisor: Pål-Tore Selbo Storli  
June 2021

Norwegian University of Science and Technology  
Faculty of Engineering  
Department of Energy and Process Engineering







---

## *Abstract*

Due to the global increase in use of renewable energy sources the need for energy storage has never been larger. The most technologically mature and economical way of storing energy today is with the application of pumped-storage hydropower (PSH). Norway has great conditions for PSH and this potential could be used to help balance the European energy grid. Therefore, there is an ongoing investigation regarding the possibility of retrofitting reversible pump turbines (RPT).

Retrofitting RPTs does pose some challenges due to cavitation. A proposed remedy to this issue is to use a booster pump (BP) in front of the RPT. By implementing a BP there may also be an increase in efficiency. The objective of this thesis is to quantify this potential efficiency difference. To do so, two RPT designs will be created. One with the BPs contribution and one without. By numerically simulating the efficiency for the two designs, comparisons can be made.

The Roskrepp power plant was used as a baseline for the input parameters when designing the geometry. To investigate the efficiencies of these designs, steady state simulations were performed with ANSYS CFX. The simulations found that the average maximum efficiency was 0.5% higher for the design with the BP. The largest maximum difference was 0.6%. Plots were also created to compare the designs at varying guide vane opening (GVO) angles. These plots further showcase that the design with the BP performs better.

The results are quite promising and displays a potential solution to how we can utilize energy storage with the application of PSH when retrofitting RPTs. However, further research should be done to confirm the accuracy of the results.



---

## *Sammendrag*

På grunn av et økende bruk av fornybare energikilder, så har behovet for energilagring aldri vært større. Den mest teknologiske modne og økonomiske metoden for lagring av energi i dag, er ved bruk av pumpekraftverk. Norge har utmerkede forhold for lagring ved bruk av pumpekraftverk og dette kan potensielt utnyttes for å balansere det Europeiske energinettverket. På grunn av dette så er det en pågående undersøkelse angående muligheten til å ettermontere reversible pumpe-turbiner (RPTer).

For å ettermontere RPTer så må problemet som er kavitasjon løses. En potensiell løsning på denne utfordringen er å bruke en boosterpumpe (BP) foran RPTen. Ved å implementere en BP så kan man potensielt oppleve en virkningsgrad økning i maskinen. Målet med denne oppgaven er å kvantifisere denne mulige virkningsgrad økningen. For å gjennomføre dette så vil to RPT design bli produsert. En med BPen sitt bidrag og en uten. Så vil numeriske simuleringer bli gjennomført for å kunne sammenligne maskinene.

Roskrepp kraftverk har blitt brukt som utgangspunkt for design av geometrien til maskinene. For å finne virkningsgraden til designene så har tidsuavhengige simuleringer blitt gjort i programvaren ANSYS CFX. Simuleringene ga et resultat som viste at den gjennomsnittlige maksimum virkningsgraden er 0.5% høyere for designet med BPen. Den største maksimale virkningsgrad forskjellen er 0.6%. Grafer ble lagd for å ytterligere vise forskjellen mellom designene ved varierende ledeskovlvinkler. Fra disse grafene kommer det tydelig frem at designet med BPen presterer bedre enn designet uten BPen sitt bidrag.

Disse resultatene er meget lovende og viser en potensiell løsning på hvordan det er mulig å få enda bedre utnytte av energilagring ved hjelp av ettermonterte RPTer. Likevel, så gjenstår det en del forskning på temaet for å forsikre seg at resultatene er til å stole på.





---

## *Acknowledgements*

I would like to thank my supervisor, Pål-Tore Selbo Storli, for giving me the opportunity to work with his incredibly exciting idea. He has been patient and helpful throughout my work and it has been fun picking his brain during discussions. Also, I would like to thank Erik Tengs for his invaluable help regarding everything CFD related.



---

## *Contents*

<b>Abstract</b>	<b>3</b>
<b>Sammendrag</b>	<b>5</b>
<b>Acknowledgements</b>	<b>7</b>
<b>Contents</b>	<b>9</b>
<b>List of Tables</b>	<b>14</b>
<b>List of Figures</b>	<b>16</b>
<b>List of Symbols</b>	<b>17</b>
<b>1 Introduction</b>	<b>1</b>
1.1 Motivation . . . . .	1
1.2 Roskrepp Power Plant . . . . .	3
1.3 Objective . . . . .	4
<b>2 Theory</b>	<b>5</b>
2.1 Hydraulic Machinery . . . . .	5

2.1.1	Reversible Pump Turbine . . . . .	5
2.1.2	Head . . . . .	6
2.1.3	Cavitation . . . . .	7
2.1.4	Performance Characteristics . . . . .	9
2.2	Computational Fluid Dynamics . . . . .	12
2.2.1	Mesh . . . . .	12
2.2.2	CFD Output Parameters . . . . .	13
<b>3</b>	<b>Methodology</b>	<b>15</b>
3.1	Designing the Geometry . . . . .	16
3.1.1	Choosing a Design Tool . . . . .	16
3.1.2	Khoj Design Process . . . . .	17
3.2	ANSYS . . . . .	23
3.2.1	ANSYS TurboGrid . . . . .	23
3.2.2	Mesh Independence Test . . . . .	25
3.2.3	Mesh Quality . . . . .	27
3.2.4	ANSYS CFX . . . . .	31
<b>4</b>	<b>Results</b>	<b>35</b>
4.1	Design 1 . . . . .	35
4.2	Design 2 . . . . .	37
<b>5</b>	<b>Discussion</b>	<b>43</b>
<b>6</b>	<b>Conclusion</b>	<b>45</b>
<b>7</b>	<b>Further work</b>	<b>47</b>

<b>References</b>	<b>49</b>
<b>A Gülich Design Method</b>	<b>53</b>
<b>B Uncertainty Analysis</b>	<b>55</b>
<b>C Grid Convergence Index</b>	<b>57</b>



---

## *List of Tables*

2.1	Empirical values for the NPSH coefficients a and b. . . . .	8
3.1	Comparing the design tools. . . . .	16
3.2	Input parameters for Khoj. . . . .	22
3.3	Node counts for design 2. . . . .	25
3.4	Node counts for design 1. . . . .	26
3.5	Mesh quality data for the runner blade and draft tube for design 1. . . . .	29
3.6	Mesh quality data for the guide vane for design 1. . . . .	29
3.7	Mesh quality data for the runner blade and draft tube for design 2. . . . .	29
3.8	Mesh quality data for the guide vane for design 2. . . . .	30
3.9	Setup parameters for the simulations. . . . .	33
4.1	Efficiency values for design 1. . . . .	35
4.2	Efficiency values for design 2. . . . .	37
4.3	Efficiency differentials (design 2 - design 1) for the two designs. . . . .	37
B.1	Uncertainty analysis results for design 1. . . . .	55
B.2	Uncertainty analysis results for design 2. . . . .	55



C.1 Grid Convergence Index results. . . . .	58
---	----

---

## *List of Figures*

1.1	The global increase in use of renewable energy sources. [1] . . . . .	2
1.2	The Roskrepp power plant [2] . . . . .	3
2.1	An overview of the components of a reversible pump turbine. [3] .	6
2.2	Velocity triangles for the inlet and outlet of an RPT. [4] . . . . .	9
3.1	Flow chart for the methods used to solve the objective. . . . .	15
3.2	Example of the main dimensions tab in Khoj. . . . .	17
3.3	The G-H plane. [5] . . . . .	19
3.4	The R- $\theta$ plane. [6] . . . . .	20
3.5	Steepness characteristics in a Q-H curve. [6] . . . . .	20
3.6	Hexahedral mesh for the runner blade and draft tube. . . . .	24
3.7	Hexahedral mesh for the guide vane. . . . .	24
3.8	Mesh independence test parameters for design 2. . . . .	26
3.9	Mesh independence test parameters for design 1. . . . .	27
3.10	Example of skewness for nodes. [7]. . . . .	28
3.11	Example of a single passage with two guide vane domains. . . . .	31
3.12	The draft tube, guide vane and blade domains. . . . .	32

4.1	$Q_{ED} - N_{ED}$ - Efficiency plot for design 1. . . . .	36
4.2	$Q_{ED} - N_{ED}$ - Efficiency plot for design 2. . . . .	38
4.3	Efficiency plotted against power output for all GVO angles at BEP. Numbers indicate GVO angle. . . . .	39
4.4	Efficiency plotted against power output for a GVO angle of 19°. .	39
4.5	Efficiency plotted against power output for a GVO angle of 22°. .	40
4.6	Efficiency plotted against power output for a GVO angle of 25°. .	40
4.7	Efficiency plotted against power output for a GVO angle of 28°. .	41
4.8	Efficiency plotted against power output for a GVO angle of 31°. .	41

---

### *List of Symbols*

**Symbols**

$\alpha$	Angle	°
$\beta$	Angle between relative and peripheral velocity	°
$\beta_b$	Blade angle	°
$c$	Absolute velocity	m/s
$c_m$	Meridional component of $c$	m/s
$c_u$	Peripheral component of $c$	m/s
$D$	Runner diameter	$m$
$e$	Error between grids	—
$\eta$	Efficiency	—
$F_s$	Safety factor	—
$G$	Length of streamline in axial direction	$m$
$g$	Gravitational constant	m/s <sup>2</sup>
$H$	Length of streamline in radial direction	$m$
$H$	Head	$m$
$h_b$	Barometric pressure	$m$
$H_S$	Suction head	$m$

$h_{va}$	Vapor pressure	$m$
$k$	Blockage caused by hub	–
$m$	Mass flow rate	$kg/s$
$n$	Rotational speed	$rpm$
$NPSH$	Net Positive Suction Head	$m$
$\Omega$	Specific speed	–
$\omega$	Angular velocity	$rad/s$
$p$	Pressure	$Pa$
$p$	Order of convergence	–
$P$	Power	$W$
$Q$	Volume flow rate	$m^3/s$
$R$	Radius	$m$
$r_{curv}$	Radius of curvature	$m$
$\rho$	Density	$kg/m^3$
$r$	Ratio of refinement	–
$\theta$	Angle in radial view	$^\circ$
$\tau$	Torque	$Nm$
$T$	Torque	$Nm$
$U$	Velocity vector $U_{x,y,z}$	
$u$	Peripheral velocity	$m/s$
$v$	Hub ratio	–
$w$	Relative velocity	$m/s$

### Abbreviation

ATM	Automatic Topology and Meshing
BEP	Best Efficiency Point

BP	Booster Pump
CFD	Computational Fluid Dynamics
CAD	Computer Aided Design
GCI	Grid Convergence Index
GUI	Graphical User Interface
GVO	Guide Vane Opening
NTNU	Norwegian University of Science and Technology
PSH	Pumped-Storage Hydropower
RPT	Reversible Pump Turbine
SST	Shear Stress Transport

### **Subscripts**

1	Turbine inlet side
2	Turbine outlet side
<i>ED</i>	Dimensionless
<i>gv</i>	Guide vanes
<i>h</i>	Hydraulic
<i>m</i>	Meridional
<i>n</i>	Hub
<i>p</i>	Poles
<i>rb</i>	Runner blades
<i>stat</i>	Static
<i>t</i>	Turbine
<i>tot</i>	Total
<i>u</i>	Peripheral



---

## Chapter I

---

### *Introduction*

#### **1.1 Motivation**

In 2021 we leave behind the warmest decade ever recorded. In 2019, we had the second warmest year ever recorded. The level of greenhouse gases in the atmosphere has never been higher than they were in 2019. [8] In 2015, the Paris agreement was signed by 196 parties. The main goal of this agreement is to limit global warming. To achieve this goal the carbon dioxide (CO<sub>2</sub>) levels, as well as the emission level of other greenhouse gases in the atmosphere, have to be reduced.

This is one reason for the large increase in use of renewable energy sources such as wind and solar. These energy production sources have the benefit of not producing greenhouse gases. However, the major drawback for these sources are their necessity for favorable weather which means that they cannot be used on demand. What this entails is the requirement for reliable energy storage technology.

The most mature and economical way of storing energy today is by pumped-storage hydropower (PSH). [9] When there is excess energy on the electrical grid, water can be pumped from a lower reservoir to an upper reservoir. And when there is a demand for energy, the same water can be run through a turbine to generate energy.

Norway has excellent conditions for PSH, as the technology requires a pair of reservoirs and a height difference. For this reason, Norway could be utilized as a green battery for Europe. However, Norway has been using hydropower as its main source of energy generation for many decades. Therefore, most of the fitting locations for the implementation of PSH are already being used. [10]

A potential solution to this may be to retrofit reversible pump turbine (RPT) units. These machines can pump water to the upper reservoir, as well as generate energy when its required. However, retrofitting these machines do provide new challenges



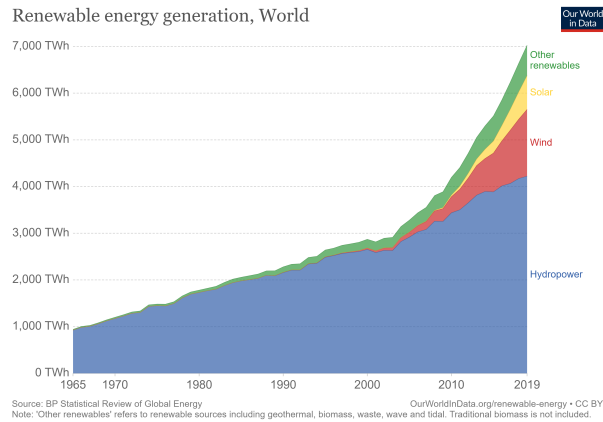


**Figure 1.1:** The global increase in use of renewable energy sources. [1]

to overcome. The main one being the need to submerge the machine further, as pumps require larger submergence than turbines due to a phenomenon called cavitation. Cavitation is the rapid creation of small cavities in the fluid that collapse which causes damages to the machine. The other issue is the fact that pumps require more pressure to overcome the height difference between the reservoirs compared to the optimal pressure a turbine should be designed for.

A possible fix for these problems is to implement a booster pump (BP) downstream of the RPT. The BP will artificially increase the pressure in the system. This means that the RPT may not have to be submerged. Also, there may be a potential efficiency increase as the RPT can be designed in a manner that is more suitable for the generating mode of the machine with regards to pressure. Quantifying this potential efficiency increase in generating mode is the main goal of this thesis.

## 1.2 Roskrepp Power Plant

Roskrepp power plant in Agder county is one of seven plants owned by Sira-Kvina. It has a single 50 MW Francis turbine in operation today. There is currently an ongoing investigation regarding the possibility of replacing the Francis turbine onsite with an RPT. It has been used as a baseline for several thesis' for students at the Waterpower laboratory which have been researching different subjects with regards to this topic.

The ongoing investigation aims to find a solution that keeps the inlet and outlet diameters equal for the RPT to the current Francis turbine that is installed. This thesis will not take this into consideration. However, it will use the rotational speed, head and discharge values for the Roskrepp power plant.



**Figure 1.2:** The Roskrepp power plant [2]

The Roskrepp power plant has a head of 83 m, the maximum flow rate is  $70 \text{ m}^3/\text{s}$ , but it is designed for a flow rate of  $50 \text{ m}^3/\text{s}$ . The rotational speed is 250 rpm. An assumption is made that the BPs contribution will give a reduction in head by 20 m for the pumping mode of the machine. It is also assumed that the machine will operate quite a lot more as a turbine than a pump, as this is the current arrangement. Because turbine mode is most essential for Roskrepp, the turbine efficiency is the most interesting to investigate.

### **1.3 Objective**

The main objective of this thesis is to quantify the efficiency difference between an RPT with and without the contribution from a BP. This will be done by designing two RPTs. By assuming that the BP contributes 20 meter in pumping mode, the geometries for the designs will be different. Then, computational fluid dynamic (CFD) simulations will be performed on both designs to find the efficiencies for both machines. The efficiencies found will then be compared. The numerical setup and design method are of course important for a task like this. However, the efficiency difference is the most interesting aspect to investigate. This is due to the fact that even though the methods used may not be optimal, if everything is done in the same manner, the efficiency differences found will still be legitimate.

For the remainder of the thesis, design 1 indicates the standard RPT and design 2 indicates the RPT with the contribution from the BP.

---

## Chapter II

---

### *Theory*

Using an RPT in combination with a BP may have rewarding results in terms of improving the efficiency. However, retrofitting an RPT does not come without certain challenges. To get a better understanding of why these challenges exist and how to quantify the potential efficiency increase, some relevant theory will be introduced.

#### **2.1 Hydraulic Machinery**

First, some theory will be provided regarding RPTs. Then common hydraulic machinery terminology which is key to understanding why this problem is important, such as head and cavitation will be described. How a BP may remedy the issues that accompanies the process of retrofitting an RPT will also be presented.

##### **2.1.1 Reversible Pump Turbine**

A reversible pump turbine is a machine that is designed as a radial pump, but when used in reverse it functions as a turbine. In its generating mode it is very similar to a Francis turbine, there are a few differences in the design approach which will be covered in greater detail later.

Some of the main benefits of a Francis turbine are the broad application range, anywhere from 20-700 meters, as well as the fact that they can reach the highest efficiencies of any type of turbine (~96%). [11] It is considered a reaction machine, meaning that it produces energy due to the pressure difference between the inlet and outlet. The energy in the water is converted to mechanical energy because of the drop in pressure. A Francis turbine also produces energy due to impulse forces from the water impinging on the runner blades.

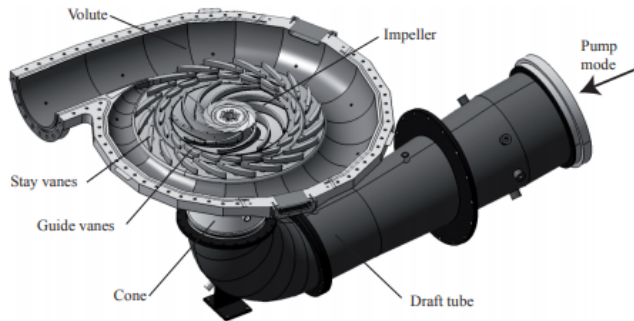


**Figure 2.1:** An overview of the components of a reversible pump turbine. [3]

To get a better understanding of how an RPT functions, the main components of an RPT will be given a short explanation:

- Volute/stay casing: The volute is where the water is transported through a decreasing cross-sectional area to maintain a constant velocity as the water is distributed equally around the stay vanes.
- The stay- and guide vanes main function are to give the water angular momentum before it reaches the runner. This is done by imparting a tangential velocity on the flow. The guide vanes can rotate, which in turn will regulate how much flow reaches into the runner, or shutting the flow off completely.
- The runner is where the potential and kinetic energy of the water is converted into mechanical energy that rotates the runner blades.
- The draft tube is a cone shaped tube designed to convert some of the kinetic energy in the flow to pressure energy. Depending on the design, it can have implications on both the efficiency of the machine and also the risk of cavitation. [12]

### 2.1.2 Head

In hydraulic machinery, the potential energy that is in water or in other words the pressure of the water, is commonly called head. It is a measurement that is given as the height of a static water column above an arbitrary point. Which is normally expressed as meters or meters of water column.

Head is crucial in design of turbines and pumps, as it will have large implications on the potential power production for turbines. For pumps, the head is the pressure the pump needs to overcome for the water to reach the required height. The head will impact both the efficiency and dimensions of the machines. The key thing to recognize is the fact that a Francis turbine in reverse will function as a pump, but not necessarily provide the required amount of head. However, an RPT designed first and foremost as a radial pump will generate enough head, but at the expense of the efficiency in generating mode.

This is the first reason that the contribution of the booster pump is interesting to study. By assuming a 20 meter contribution from the booster pump in pumping mode, it is possible to design the RPT in a way that is more favorable for its generating mode.

### 2.1.3 Cavitation

Cavitation is a phenomenon in hydraulic machinery that can cause critical damage. It is water that essentially boils due to low pressure. The water evaporates creating small cavities that burst as rapidly as they are formed, these bursts creates shocks which in the long term can and will cause damage to the machinery. If left unchecked, it will eventually lead to failure of the machine.

If the local static pressure becomes less than the vapor pressure of the water, cavitation will occur. Obviously, due to the severe consequences this phenomenon may inflict, it is of paramount importance to avoid the conditions required for it to happen at all. One way to ensure that there will be no cavitation is to submerge the runner below the lower reservoir. This has the effect of increasing the static pressure at the turbine outlet side which means there will be a lower or no risk of cavitation.

To calculate the level of submergence needed to avoid cavitation it is common practice to use the characteristic parameter: Net Positive Suction Head (NPSH). The definition of NPSH is the absolute pressure at the turbine outlet, minus the vapor pressure.

$NPSH_R$  defines how large of an submergence is required to avoid cavitation. It can be calculated in the following way:

$$NPSH_R = a \frac{c_{m2}^2}{2g} + b \frac{u^2}{2g} \quad (2.1)$$

a, b - Coefficients of submergence

$c_m$  - Meridian component of the absolute velocity [m/s]

$u$  - Peripheral velocity [m/s]

The coefficients of submergence depend on the speed number, the blade geometry and the number of blades. [13] They are determined empirically and their ranges can be seen in Table 2.1.

Parameter	Turbines	Pumps
a	$1.05 < a < 1.15$	$1.60 < a < 2.00$
b	$0.05 < b < 0.15$	$0.20 < b < 0.25$

**Table 2.1:** Empirical values for the NPSH coefficients a and b.

$NPSH_A$  states how large the NPSH available for the plant is with regards to the level of submergence for the machine. It is defined in the subsequent manner:

$$NPSH_A = -H_s + h_b - h_{va} \quad (2.2)$$

$H_s$  - The necessary submergence of the runner

$h_b$  - Barometric pressure

$h_{va}$  - Vapor pressure

These are all expressed in meters.

Finally, to avoid cavitation there is one demand that needs to be fulfilled and that is described in Equation 2.3:

$$NPSH_A > NPSH_R \quad (2.3)$$

The second reason the BPs contribution is exciting to investigate is the fact that the safety margin required to avoid the risk of cavitation states that Equation 2.3 has to be true. This margin will be smaller when an RPT is operating in pump mode. Therefore, the standard solution is to submerge the machine. However, by increasing the pressure with a BP the  $NPSH_A$  will become larger and thus the required submergence will be smaller or possibly not necessary at all.

### 2.1.4 Performance Characteristics

In the following section, the Euler equations will be presented to showcase how the efficiency of an RPT can be calculated. Also, the dimensionless parameters  $Q_{ED}$  and  $N_{ED}$  will be introduced. As well as a way to calculate the power output for a turbine.

The Euler equations are fundamental equations that govern the power and efficiencies for turbomachinery. They are also used when designing pumps and turbines. Equation 2.4 is important for both of these reasons.

$$\eta_h \rho g Q H = \rho Q (u_1 c_{u1} - u_2 c_{u2}) = \omega T \quad (2.4)$$

Where  $\eta_h$  is the hydraulic efficiency of the machine,  $\rho$  is the density of the fluid [ $kg/m^3$ ],  $g$ ,  $Q$  and  $H$  are the gravitational constant [ $m/s^2$ ], volume flow rate [ $m^3/s$ ] and head [ $m$ ] respectively.  $u$ ,  $c_u$  and  $\omega$  are the peripheral [ $m/s$ ], meridian [ $m/s$ ] and rotational [ $rad/s$ ] velocities. And finally  $T$ , which is the torque [ $W$ ].

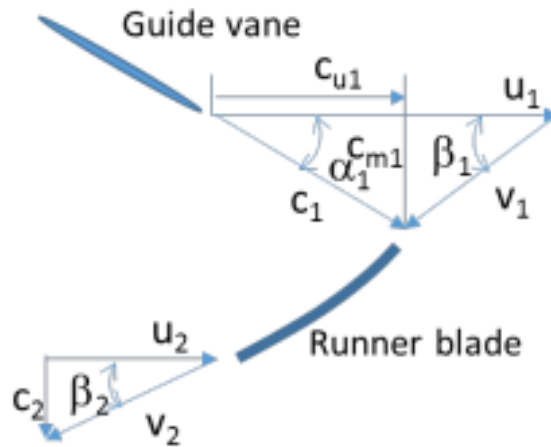


**Figure 2.2:** Velocity triangles for the inlet and outlet of an RPT. [4]

When isolating the hydraulic efficiency we can rearrange Equation 2.4 into the two following ways:



$$\eta_h = \frac{(u_1 c_{u1} - u_2 c_{u2})\omega}{gH} \quad (2.5)$$

This efficiency is the ratio of how much theoretical energy there is in the water, to how much energy is produced by the turbine. This equation does not, however, account for the hydraulic losses that will be present in the waterways. Equation 2.5 is also commonly used when designing an RPT. It is standard practice to set  $\eta_h = 0.96$ , by doing so it is possible to find the values in the velocity triangles. [13] The second way of expressing the efficiency is shown in Equation 2.6:

$$\eta_h = \frac{\omega T}{gH\rho Q} \quad (2.6)$$

This equation is more useful for our case which will be demonstrated in the following chapter, as it allows us to find the efficiency for an RPT numerically.

The power output that the machines will be able to produce is also important as it will be used to compare the two designs in the results section. It is defined in the following manner:

$$P = \eta_t \times \rho \times g \times Q \times H \quad (2.7)$$

Here, P, is power output [W],  $\eta_t$  is the turbine efficiency,  $\rho$  is the density of the water [ $kg/m^3$ ], g is the gravitational constant [ $m/s^2$ ], Q the volume flow [ $m^3/s$ ] and H is head [m].

When designing hydraulic machinery it is useful to operate with dimensionless numbers and reduced values. Reducing parameters is achieved by dividing said parameter with the maximum water velocity for the given system with:  $\sqrt{2gH}$ . This value represents all the available energy for a system if there were no losses.

A key parameter for turbomachinery is the speed number,  $\Omega$ . This speed is obtained by combining the reduced rotational speed with reduced flow rate and is described by the following equation: [12]

$$\Omega = \omega \sqrt{\frac{Q}{gH}} = \frac{\omega}{\sqrt{2gH}} \sqrt{\frac{Q}{\sqrt{2gH}}} = \frac{\omega Q^{1/2}}{(2gH)^{3/4}} \quad (2.8)$$

This is a dimensionless number. All the parameters in Equation 2.8 are nominal values corresponding to the Best Efficiency Point (BEP). [14] Some references also use the follow definition:

$$\Omega = \frac{\omega Q^{1/2}}{(gH)^{3/4}} \quad (2.9)$$

$Q_{ED}$  and  $N_{ED}$  are dimensionless variables that are used for similarity analysis and also portrays the performance characteristics for turbomachinery. These parameters say something about the discharge- and speed factor for the machine. They can provide an overview of how a machine will operate at various amounts of flow and rotational speeds. Also, by altering the rotational speed this can represent variations in head, which normally can be difficult to model for. This is because a variation in head has the same effect as a variation in speed, since the runner is rotating either too fast or slow compared to the head. [12] This relationship can also be seen in Equation 2.11. They are defined in the following manner:

$$Q_{ED} = \frac{Q}{D_2^2 \sqrt{gH}} \quad (2.10)$$

$$N_{ED} = \frac{nD_2}{\sqrt{gH}} \quad (2.11)$$

Rearranging these two equations and substituting them into Equation 2.9 we get the following important relation regarding the speed number, discharge factor and speed factor:

$$\Omega = N_{ED} \times \sqrt{Q_{ED}} \quad (2.12)$$

## 2.2 Computational Fluid Dynamics

Computational fluid dynamics is the application of computers to numerically solve problems that would be near to impossible to solve analytically. CFD has a wide range of application areas such as fluid flows, heat transfer and chemical reactions. In hydrodynamics for example, it can be used to predict the effects of cavitation, erosion or to gain insight into the performance characteristics of a machine.

There are several options for CFD tools currently. For this thesis ANSYS CFX was chosen for the following reasons: It is user friendly, has excellent documentation online and is licensed by NTNU.

### 2.2.1 Mesh

ANSYS CFX solves the Navier-Stokes equations for every node which makes up a larger mesh grid. The accuracy of a CFD simulation is heavily influenced by the number of nodes in the grid. By making the nodes smaller and therefore increasing the amount of nodes necessary to cover the whole grid, the accuracy will improve at the cost of computational resources. [15] For these reasons, it is key to produce a mesh that is suitable for the given problem.

To achieve the goal of creating an adequate mesh that produces results that are as accurate as deemed necessary with the smallest computational costs, a mesh independence test is performed. A mesh independence test is generally considered the most straightforward approach and is arguably the most reliable way of quantifying the numerical error. [16]

A mesh independence study is performed by producing a mesh for a given steady state simulation, which then three independent criteria has to be met:

1. The simulation converges and the residual RMS levels has reached an acceptable level. Usually a value below  $10^{-4}$ .
2. Points of interest are monitored during simulation. These monitor points have to reach a steady solution.
3. The domain has imbalances of less than 1%.

Then, this process is repeated for coarser and finer meshes. The coarsest mesh that fulfills these criteria is chosen, this is to reduce the computational time and resources required as much as possible.

### 2.2.2 CFD Output Parameters

In this thesis, the efficiency is the key parameter to investigate and assess. In subsection 2.1.4 how the efficiency is normally calculated was presented. However, to find the efficiency from a numerical simulation, several parameters have to be defined and calculated. These parameters are: head, pressure and torque. It is also some of these parameters that are chosen as monitor points in the mesh independence test.

$$H = \frac{p_{tot1} - p_{tot2}}{\rho g} \quad (2.13)$$

$p_{tot}$  is the pressure [Pa] of the fluid at the entrance and exit of the simulation if the fluid was brought instantaneously to rest. The definition of  $p_{tot}$  is given here:

$$p_{tot} = p_{stat} + \frac{1}{2}\rho(U \cdot U) \quad (2.14)$$

Here,  $p_{stat}$  is the static pressure and  $U$  is the velocity vector in the x, y and z-direction.

Torque, the rotational forces in the machine, is defined in the following way:

$$\tau_{tot} = \tau_{blade} + \tau_{hub} + \tau_{shroud} \quad (2.15)$$

The hub and shroud are the walls of the runner.

$\omega$  is automatically calculated by ANSYS, but is defined like this:

$$\omega = \frac{2\pi n}{60} \quad (2.16)$$

Where  $n$  is the rotational velocity [rpm].

When inserting for  $\tau$ , head and volume flow from Equation 2.6 we get:

$$\eta_h = \frac{\tau_{tot}\omega}{(p_{tot1} - p_{tot2})\frac{m}{\rho}} \quad (2.17)$$

Where  $m$  is the mass flow rate of the fluid [kg/s].

The efficiency in Equation 2.17 is the main goal of this thesis to find as accurately as possible for both RPT designs.

---

## Chapter III

---

### *Methodology*

In this chapter the methods used for solving the problem will be described. Theory that is relevant for the choices that were made during this process will also be presented and explained. Below is an illustration of a flow chart which gives an overview of the steps taken to arrive at a solution. All the steps in the flow chart will be explained in greater detail in this chapter.

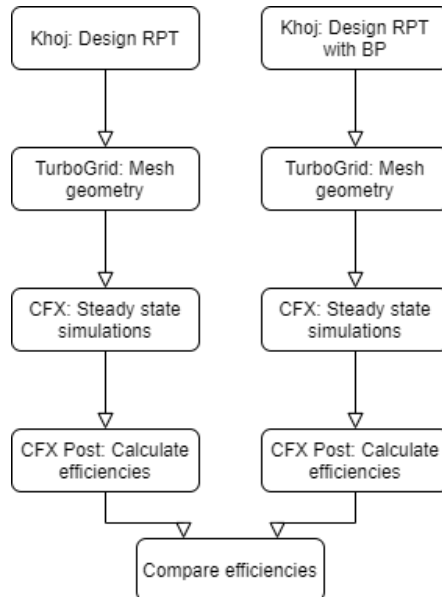


**Figure 3.1:** Flow chart for the methods used to solve the objective.

## 3.1 Designing the Geometry

### 3.1.1 Choosing a Design Tool

Khoj is a graphical user interface (GUI) design software programmed in MatLab. It was made by former students at the Waterpower Laboratory at the Norwegian University of Science and Technology (NTNU). Khoj was made as a design tool for Francis turbines, but by varying certain design parameters it can also be used to design RPTs. In Khoj it is possible to design the geometry for the runner, guide vanes and spiral casing. The resulting design files can then be imported into CFD software such as ANSYS. To describe why Khoj was chosen as a design tool in this thesis, other options for designing the geometry of an RPT will be given a brief presentation.

The method that allows the user the most freedom with regards to design choices is computer aided design (CAD) software such as AutoDesk Inventor, DesignModeler or SolidWorks. With CAD software the only limiting factors are the users time and skills. In these programs one can design parts in exactly the manner as one requires, as long as the experience of the user is up to the task. Modelling the parts of RPTs is quite a time-consuming endeavour, even for experienced users.

Another way of designing the geometry for RPTs is with specialized design software such as ANSYS BladeGen. BladeGen is an interactive design tool for turbomachinery. In some ways it resembles Khoj, with the key difference being that it is more complex and requires more knowledge regarding the software to use adequately. It is however, not as constrained as Khoj, meaning the user has more freedom regarding design choices. A summarized description of these design choices are presented in the following table:

Design tool	Positives	Negatives
CAD Software	Allows experienced users to design geometry without any constraints	Time-consuming and heavily reliant on knowledge and experience with software
Khoj	Very user friendly, requires little to no knowledge regarding the software	Constrained by the available design choices
BladeGen	Much documentation online, allows a greater deal of customization than Khoj	Not as user friendly as Khoj, requires knowledge of software to create satisfying designs

**Table 3.1:** Comparing the design tools.

The key goal of this thesis is to quantify the efficiency difference between the two designs. Any of these design options still allows enough freedom in design choices to portray the contribution of a BP. Therefore, Khoj was chosen as this requires the least amount of time and prior knowledge to sufficiently design the RPTs. The focal point for designing the RPTs is that the method for both are as similar as possible. Quantifying the efficiency difference is still possible with the chosen design method.

### 3.1.2 Khoj Design Process

Designing an RPT in Khoj is a streamlined processed. The program is made up by several tabs that walks the user through the necessary steps. In the end, the chosen parameters can be viewed, as well as the possibility of exporting the geometry in the form of curve files to fitting CFD software such as ANSYS.

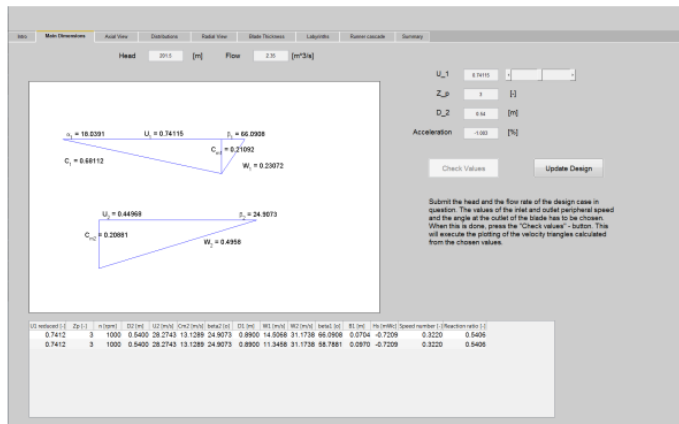


Figure 3.2: Example of the main dimensions tab in Khoj.

The main dimensions for the RPT are entered in the second tab of Khoj, as seen in Figure 3.2. These are the following dimensions: Head, volume flow,  $u_1$ , number of poles,  $D_2$  and percentage of acceleration through the runner. The reduced inlet peripheral velocity  $u_1$  is nearly equal to one, in this case it chosen as 0.95. Values close to one provides steep pump characteristics which are favorable. The reason being that steep characteristics ensures the possibility of operating at many different head values without needing to change the volume flow significantly. [6, 17]  $Z_p$  is the number of poles in the generator. This value is 12 which is equal to the amount for the generator at Roskrepp. The acceleration through the runner is chosen to



be zero. It is common to design turbines and pumps with acceleration as this is favorable for the reduction of stall in the airfoils. In RPTs however, it is desirable to design the machine without acceleration. This is due to the fact that acceleration in one direction will cause deceleration in the opposite direction. [6]

The turbine outlet diameter  $D_2$  [m], is calculated with the following equation:

$$D_2 = 2.9 \times \sqrt[3]{\frac{Q}{nk_n \tan \beta_2} \left(1 + \frac{\tan \beta_2}{\tan \alpha_2}\right)} \quad (3.1)$$

The subscript 2 denotes the turbine outlet. Beta and alpha are angles.  $n$  is the rotational speed [rpm].  $k_n$  is the blockage caused by the hub. This equation is taken from Gülich's book Centrifugal Pumps. Gülich's design process for pumps is described in greater detail in Appendix A.

Next in the design process is to design the runner blades. The procedure begins by shaping the blade in the axial view, then the radial view and finally, the blade is plotted in three dimensions. The  $U \times c_u$  energy distribution was flattened at both ends by making the blades longer. Longer blades can increase the risk of backflow and stability problems, so the blades were also stretched to counteract this. [17] Runners that are designed for high  $NPSH_A$  can be optimized better for high efficiency. [18] A distribution has to be chosen for all streamlines. By choosing a  $U \times c_u$  distribution, the distribution of the blade angle will be different for every streamline. The blade angles can be found by using the following equation:

$$\beta_B = \arctan\left(\frac{c_m}{u - c_u}\right) \quad (3.2)$$

To change the coordinates from the axial view to the radial view, a common procedure is to introduce a G-H plane. G is the length of streamlines in the axial view and H is the length of a streamline in the radial view. This procedure is normal to use for the design of centrifugal pump impellers. [19, 20]

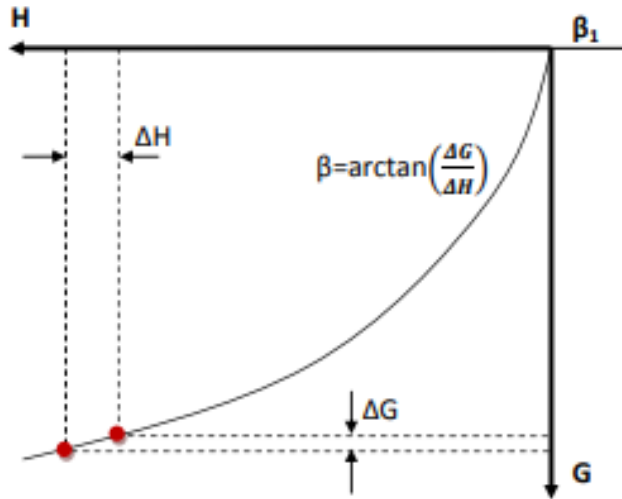


**Figure 3.3:** The G-H plane. [5]

Calculating the values of G and H are done in the following manner:

$$G_{i,1} = G_{i-1,1} + \sqrt{(R_{i-1,1} - R_{i,1})^2 + (Z_{i-1,1} - Z_{i,1})^2} \quad (3.3)$$

Which gives the length of a streamline in meters. R and Z are values from the axial view. G is equal to zero at the inlet.

$$\Delta H = \frac{\Delta G}{\tan \beta} \quad (3.4)$$

This process has to be repeated for every streamline, then the G-H plane can be plotted and the radial view can be established by Equation 3.5. This relationship is illustrated in Figure 3.4

$$d\theta = \frac{\Delta H}{R} \quad (3.5)$$

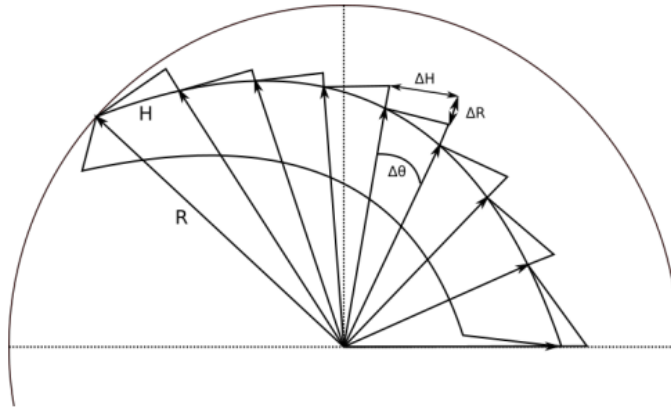


**Figure 3.4:** The  $R-\theta$  plane. [6]

Next, the number of runner blades has to be determined. According to Gülich, eight or more blades are normally not recommended due to the stability of the  $Q-H$  curve. If the operating range is not narrow, Gülich recommends 5-7 blades. For cases where a stable  $Q-H$  curve is not needed, 9 blades can also be used.

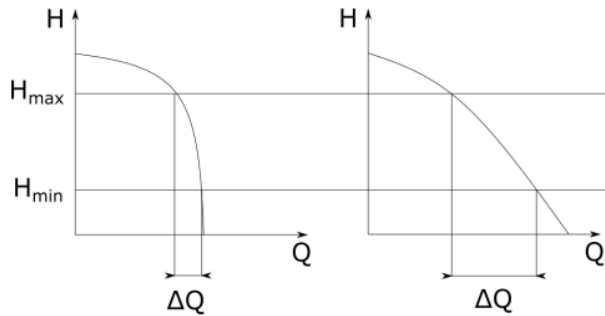


**Figure 3.5:** Steepness characteristics in a  $Q-H$  curve. [6]

Backflow is the other factor that has to be considered when choosing the number of runner blades. To understand how to circumvent backflow from appearing in the runner, Equation 3.6 has to be investigated:

$$\frac{\partial w}{\partial n} = -2\omega - \frac{w}{r_{curv}} \quad (3.6)$$

Here  $\omega$  is the rotational velocity,  $w$  is the relative velocity along a line,  $n$ , normal to the streamlines.  $r_{curv}$  is the radius of the curve of the blade surface. [21]

The relative velocity at the pressure side of the blade cannot be negative or backflow will occur. The relative velocity increases with the flow rate, the maximum velocity is found at full load. A decrease in  $\Delta w$  will cause narrow channels and in turn create the need for an increase in the number of runner blades. Therefore at some part loads there will be backflow. The solution is to choose the amount of runner blades for a certain design load. This is typically chosen to be 80% of the BEP flow rate. [21] To calculate the number of runner blades the relative velocity is set to zero at the inlet on the pressure side. Flow rate is 80% of BEP. The value for  $c_u$  is chosen as designed and  $c_m$  is found from continuity. The distance  $\Delta n$ , which is the distance from the middle of the channel to the blade is found from Equation 3.7. [21]

$$\Delta n = \frac{1}{\frac{\partial w}{\partial n}} \Delta w = const \times \Delta w \quad (3.7)$$

Then finally, the number of blades is found from the following equation:

$$Z_{rb} = \frac{Circumference}{ChannelWidth} = \frac{\pi D_1}{2\Delta n} \quad (3.8)$$

The final settings that have to be configured in Khoj are related to the guide vanes. Gülich states that a suitable selection for the number of guide vanes is a number that does not share a common integer multiplier with the number of runner blades. [18] The flow from the guide vane outlet to the runner inlet is unaffected so free vortex theory can be applied to find the velocity components. The guide vane outlet angle can be found from the velocity triangle.

$$\tan \alpha_{gvo} = \frac{c_m}{c_u} \quad (3.9)$$

Generally, it is considered favorable for the guide vanes to be long as this will ensure the flow is guided better. However, this will account for larger friction

losses. [17] The number of guide vanes are selected so that no water can enter the runner in its closed position. It is common that the length overlaps around 10-15 %. [17, 21] The vanes are shaped as airfoils to decrease flow losses.

Below are the table containing the input parameters that were used for both designs in Khoj. The runner blade, draft tube and guide vane profiles created were exported to ANSYS.

Parameter	Description	Design 1	Design 2	Unit
Q	Volume flow rate	50	50	$m^3$
H	Head	83	63	m
$u_1$	Reduced inlet peripheral velocity	0.95	0.95	-
$\beta_2$	Outlet blade angle	23.8	28.3	°
$u_2$	Outlet peripheral velocity	29.7	27.8	m/s
$Z_p$	Numbers of pole pairs in generator	12	12	-
$D_2$	Turbine outlet diameter	2.27	2.12	m
acc	Acceleration through runner	0	0	%
$Z_{rb}$	Number of runner blades	7	7	-
$Z_{gv}$	Number of guide vanes	17	17	-

**Table 3.2:** Input parameters for Khoj.

## 3.2 ANSYS

For the reasons mentioned in section 2.2, ANSYS was chosen to perform the meshing and numerical simulations required to solve the main objective for this thesis. ANSYS provides a great project overview in the form of Workbench that allows bidirectional communication between CAD systems. In Workbench it is easy to set up schematic views over projects. Workbench provides an easy way of auto-updating project features across software modules. Also, data can easily be transferred between said modules and it also makes it possible to run many simulations by varying certain input parameters such as guide vane angles and rotational speeds.

### 3.2.1 ANSYS TurboGrid

After the curve files were produced in Khoj, they were then imported into ANSYS TurboGrid. TurboGrid is a tool for meshing of turbomachinery components. ANSYS claims it automatically produces high quality meshes. TurboGrid has been used with good results previously, therefore the claim is assumed to be valid. [21–24]

The hexahedral meshes are created with an inbuilt meshing algorithm called Automatic Topology and Meshing (ATM). TurboGrid automatically refines the mesh in regions of interest. For example, the amount of nodes will be larger for the runner blade than they would be for the draft tube. This is also illustrated in Figure 3.6.

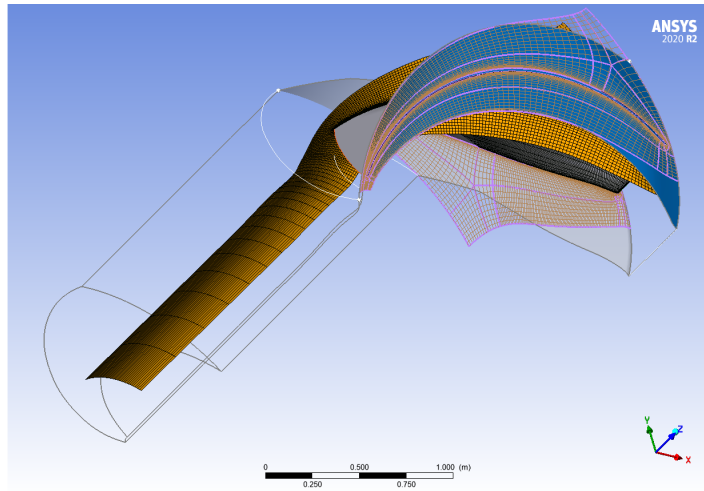


**Figure 3.6:** Hexahedral mesh for the runner blade and draft tube.

The simulation domain was divided into three parts, but meshed in two. The runner blade and draft tube were meshed together. The guide vane was meshed by itself. The guide vane was also meshed for  $\pm 3$  degrees and  $\pm 6$  degrees.

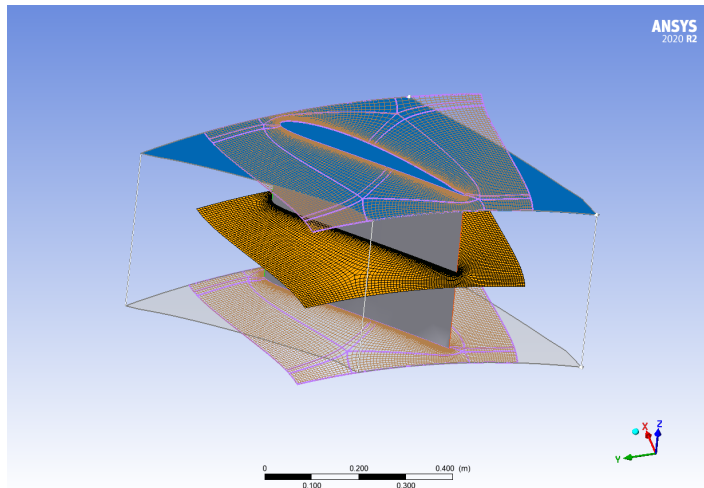


**Figure 3.7:** Hexahedral mesh for the guide vane.

### 3.2.2 Mesh Independence Test

To ensure that the results produced are achieved as fast as possible with the required level of accuracy, a mesh independence test was performed for both designs. The reasoning for why this is important and how this is done was explained in subsection 2.2.1.

The mesh independence tests were performed for five different mesh sizes. The key parameters that were chosen to perform the mesh independence test were: torque, pressure and hydraulic efficiency. In this case, the pressure used was the difference in pressure of the fluid if it was instantaneously put to rest between the in- and outlet. The reason being that this pressure value is key for finding the efficiency, as explained in subsection 2.2.2. The mesh sizes varied from 140 000 - 2 200 000 nodes.

Global size factor	Number of nodes
0.5	142 422
0.6	228 985
0.75	449 161
1	1 010 142
1.25	1 941 108

**Table 3.3:** Node counts for design 2.

The global size factor feature in TurboGrid was used to automatically adjust the refinement of the meshes. If the meshes produced by TurboGrid created errors in the mesh quality then refinements were made in the boundary layer refinement control panel in TurboGrid. This was done to ensure the mesh independence test results were reliable. The mesh size that was chosen for the simulations was the one with a global size factor of 0.75 and 449 161 nodes. Below are graphs displaying the output values vs. node count. The deviations from the finest mesh were 0.144% for the efficiency, 0.064% for the torque and 0.211% for the pressure difference.



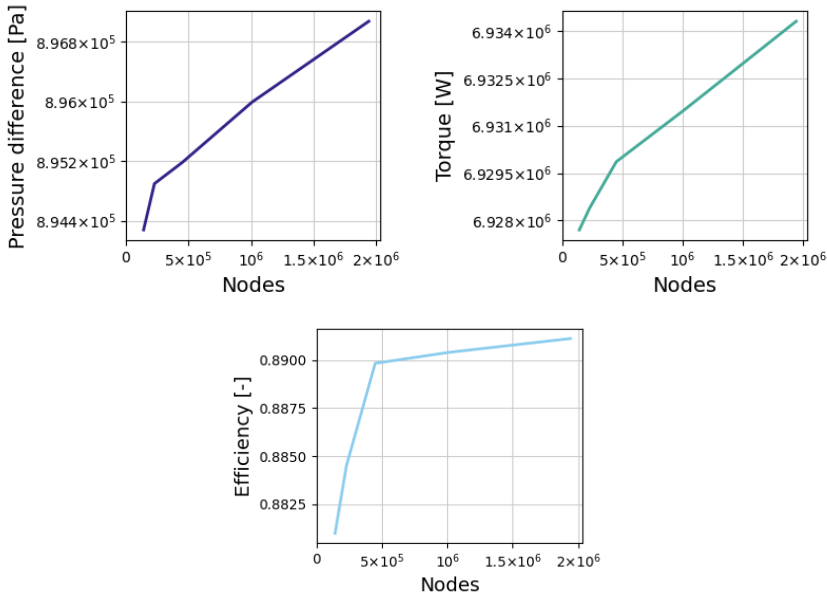


**Figure 3.8:** Mesh independence test parameters for design 2.

Global size factor	Number of nodes
0.5	167 191
0.6	267 101
0.75	495 679
1	1 138 684
1.25	2 205 175

**Table 3.4:** Node counts for design 1.

For design 1, the mesh with a global size factor of 0.75 was also chosen. Here the deviations from the finest mesh were 0.25% for the efficiency, 0.138% for the torque and 0.348% for the pressure difference.

To ensure that these deviations are acceptable, a grid convergence index (GCI) was performed. The results of the GCI showed that these deviations were indeed satisfactory. This process is described in Appendix C.

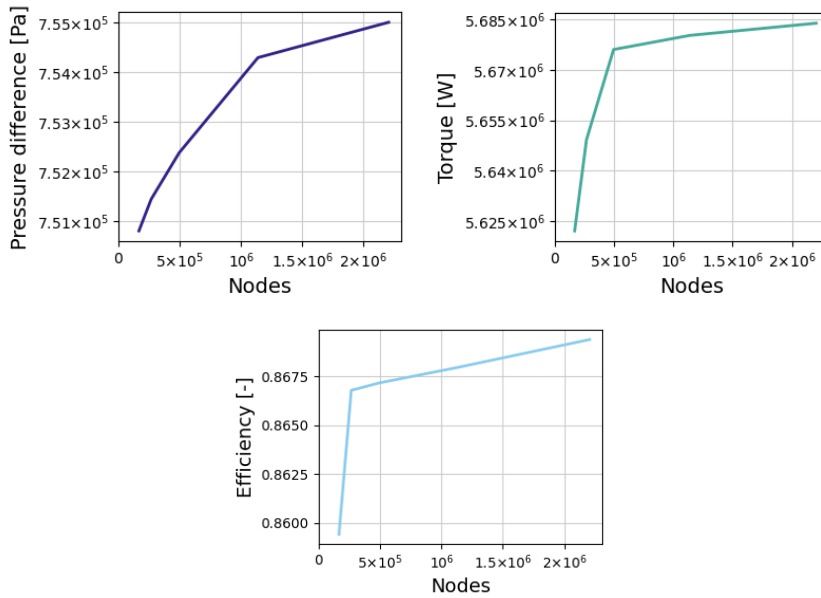


**Figure 3.9:** Mesh independence test parameters for design 1.

### 3.2.3 Mesh Quality

TurboGrid provides a feature that automatically provides feedback on the quality of the meshes that were produced. If the values are below the accepted limits, TurboGrid will highlight these areas and allow the user to improve on the mesh. In the following section, tables that detail the mesh qualities for the guide vanes and blades for both designs are given. The results show that the meshes produced are at an acceptable level.

For these tables to provide insight, the definition of these measurements have to be described.

The face angles are the angles between edges of the faces that touch the node. For every face on the node, the angle between the edges are calculated to find the largest angle. This returned maximum value can be considered a measurement of skewness for the node. Lower skewness implies better mesh quality. Skewness above 0.85 is generally considered unacceptable. [25]

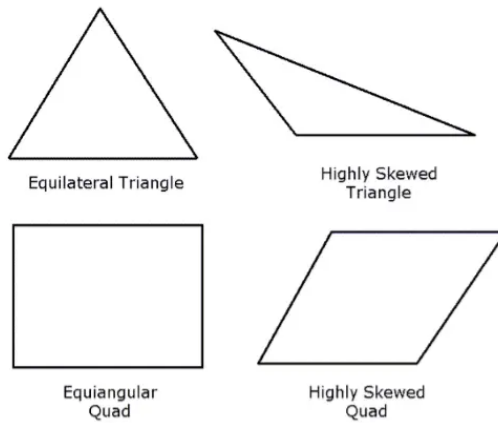


**Figure 3.10:** Example of skewness for nodes. [7].

The element volume ratio is the ratio between the maximum and minimum volume of elements that touch a node. This measurement can be used as the local expansion factor. [25]

The minimum volume measurement is used to ensure that there is no presence of negative volumes. The value is the minimum volume for an element touching any of the nodes. [25]

The edge length ratio is the ratio of the longest edge for a face divided by the shortest edge. This is calculated for every face and the largest ratio is returned. This measurement can be viewed as the aspect ratio. [25]

The connectivity number is the number of elements that touch a node. High numbers for this value can have an adverse effect on the speed of structured solvers. For unstructured solvers however, this value is not important. [25]

<b>Mesh measurement</b>	<b>Value</b>	<b>% Bad</b>
Minimum Face Angle	21.03 °	0.0
Maximum Face Angle	158.9 °	0.0
Maximum Element Volume Ratio	7.29	0.0
Minimum Volume	$1.96 \times 10^{-10} m^3$	0.0
Maximum Edge Length Ratio	415.5	0.0
Maximum Connectivity number	10	0.0

**Table 3.5:** Mesh quality data for the runner blade and draft tube for design 1.

<b>Mesh measurement</b>	<b>Value</b>	<b>% Bad</b>
Minimum Face Angle	45.7 °	0.0
Maximum Face Angle	127.9 °	0.0
Maximum Element Volume Ratio	3.77	0.0
Minimum Volume	$1.12 \times 10^{-11} m^3$	0.0
Maximum Edge Length Ratio	358.3	0.0
Maximum Connectivity number	10	0.0

**Table 3.6:** Mesh quality data for the guide vane for design 1.

<b>Mesh measurement</b>	<b>Value</b>	<b>% Bad</b>
Minimum Face Angle	28.11 °	0.0
Maximum Face Angle	151.9 °	0.0
Maximum Element Volume Ratio	6.03	0.0
Minimum Volume	$7.45 \times 10^{-10} m^3$	0.0
Maximum Edge Length Ratio	196.29	0.0
Maximum Connectivity number	10	0.0

**Table 3.7:** Mesh quality data for the runner blade and draft tube for design 2.

---

<b>Mesh measurement</b>	<b>Value</b>	<b>% Bad</b>
Minimum Face Angle	44.35 °	0.0
Maximum Face Angle	128.03 °	0.0
Maximum Element Volume Ratio	3.929	0.0
Minimum Volume	$2.36 \times 10^{-11} m^3$	0.0
Maximum Edge Length Ratio	232.72	0.0
Maximum Connectivity number	10	0.0

---

**Table 3.8:** Mesh quality data for the guide vane for design 2.

### 3.2.4 ANSYS CFX

Steady state simulations were run for both designs in ANSYS CFX. The software offers a specific approach called Turbo Mode which easily sets up the boundary conditions and interfaces between the components. Rotational periodicity was applied to save computational time and resources, meaning the simulations were only done on a single passage. Then, the results are copied around. The simulations were run for several guide vane opening (GVO) angles as well as varying rotational speeds. To keep the pitch ratio close to unity, two guide vane domains were used for a single passage. The reason being that a pitch ratio close or equal to one is usually more favorable for the accuracy of transient simulations. [26] It was intended to run transient simulations to further verify the accuracy of the results, but due to time constraints this was not achieved.

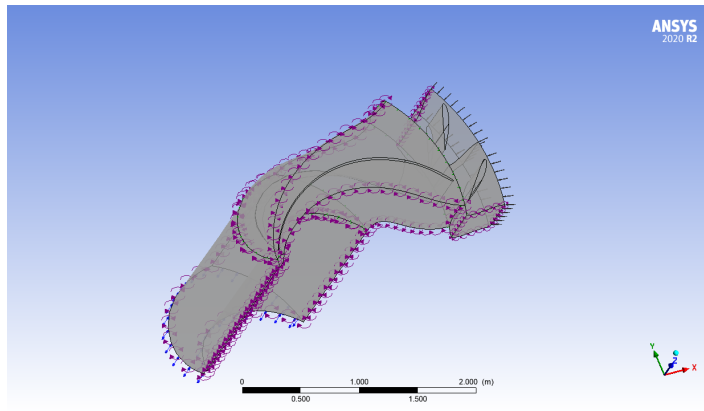


**Figure 3.11:** Example of a single passage with two guide vane domains.

ANSYS CFX solves the Reynolds-Averaged Navier Stokes equations for mass, momentum and energy. It applies the finite volume method. The solution domain is divided into several small control volumes. The equations are applied to each control volume, as well as the solution domain as a whole. The turbulence model that was used for all the simulations was the shear stress transport (SST) model. The SST turbulence model is a two equation eddy-viscosity model that combines the  $k-\omega$  and  $k-\epsilon$  models. The  $k-\omega$  model is excellent for simulation of flow in the viscous sub-layer and the  $k-\epsilon$  model is ideal for flow away from walls. [27] Menter suggests this turbulence model for adverse pressure gradient flows. [28] The SST model has also been previously used in [23, 24, 29] with fine results. It is also recommended by the ANSYS CFX Rotational Machinery Modeling Guide. [26]. Chirag Trivedi has also conducted transient CFD simulations with the SST model

achieving good results. [30]

The interfaces between the rotating and stationary domains are all modeled as Stage (Mixing-Plane). The other interface models are set to rotational periodicity.

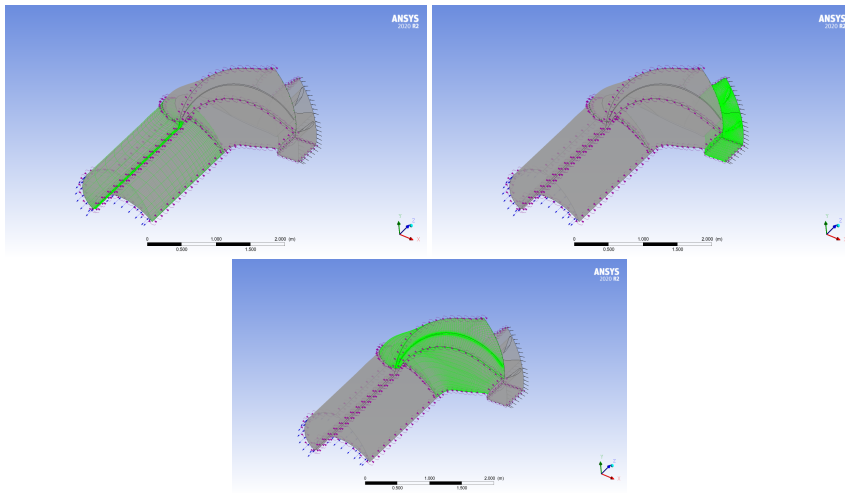


**Figure 3.12:** The draft tube, guide vane and blade domains.

The inlet boundary condition was defined as a simple homogeneous velocity profile, with specifications listed in Table 3.9. The outlet boundary condition was set as an opening with 0 [Pa] pressure outlet, the velocity direction was set to normal to boundary condition. Opening outlet boundary condition allows for flow in both directions. The boundary condition for the walls were all set to smooth surface with no slip. With one exception being the shroud, which is set as a counter-rotating wall.

Table 3.9 summarizes the setup for the simulation runs for both designs. These settings were all equal for both designs, guide vane angles and the different rotational speeds to ensure the results would be comparable.

Parameter	Description
Domains	1: Stationary inflow, two guide vanes 2: Rotating, one runner blade 3: Stationary, draft tube
Mesh	Reference pressure: 1 atm Hexahedral, approximately 450 000 and 500 000 nodes
Simulation type	Steady state
Turbulence model	SST
Interfaces	Inflow-Runner and Runner-Draft: General connection, Stage (Mixing Plane), Mesh connection: GGI Inflow, draft and runner periodic: Rotational periodicity, Mesh connection: GGI
Boundary conditions	Inlet: Mass flow rate: 7143 kg/s per passage. Seven passages. Direction: Cylindrical components (a, r, t): 0, -1, -1. Turbulence: Medium intensity 5% Outlet: Opening, 0 Pa pressure. Direction: Normal to boundary condition. Turbulence: Medium intensity 5%. Walls: Smooth walls with no slip condition. Shroud: Counter-rotating wall
Fluid	Water at 278 K, Heat transfer: Isothermal
Solver control	Advection Scheme: High Resolution
Convergence control	Min-max. iterations 100-400, Physical timescale: Auto Timescale, Length Scale Option: Conservative, residual target (RMS): 1E-4
Run type	12 Cores AMD Ryzen 9 3900X @ 3.80 GHz, 32 GB ram, double precision

**Table 3.9:** Setup parameters for the simulations.





---

## Chapter IV

---

### *Results*

In this chapter the numerical results are presented. This includes the maximum efficiencies for both designs as well as a comparison between their average maximum efficiencies. The rotational speeds were varied from 200-410 RPM with an interval of 10, and the GVO angles were also regulated in the range of  $\pm 3^\circ$  and  $\pm 6^\circ$  from the BEP. To showcase the performance characteristics for both designs, 3D  $Q_{ED} - N_{ED}$  - Efficiency plots were produced with Python. These parameters were found in CFX Post by using the equations presented in subsection 2.1.4 and subsection 2.2.2. Uncertainty analysis was also performed for these monitor points. The results of this analysis are presented in Appendix B.

#### 4.1 Design 1

For the first design, the maximum efficiency was found to be 94.78%. At a GVO angle of  $25^\circ$  which is the BEP and at a rotational speed of 340 rpm. The  $Q_{ED}$  and  $N_{ED}$  values for the maximum efficiency are 0.396 and 0.425 respectively. The overall average efficiency was 85.4% for the whole design. The average maximum efficiency was found to be 94.3%. This was the average maximum efficiency for each GVO angle.

<b>GVO angle</b>	<b>Min. efficiency</b>	<b>Max. efficiency</b>
19°	75.2%	94.2%
22°	79.1%	94.73%
25°	76.7%	94.78%
28°	74.5%	94.5%
31°	71.1%	93.1%

**Table 4.1:** Efficiency values for design 1.

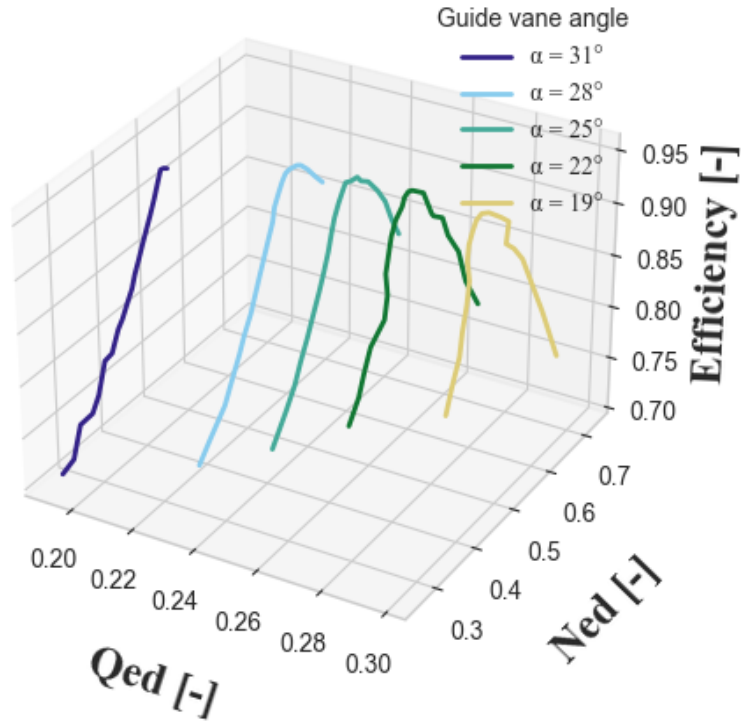


Figure 4.1:  $Q_{ED}$  -  $N_{ED}$  - Efficiency plot for design 1.

## 4.2 Design 2

For the second design, the maximum efficiency was found to be 95.4%. At a GVO angle of 22° and at a rotational speed of 320 rpm. The  $Q_{ED}$  and  $N_{ED}$  values for the maximum efficiency point are 0.331 and 0.413 respectively. The overall average efficiency was 87.1% for the whole design. The average maximum efficiency was found to be 94.8%.

GVO angle	Min. efficiency	Max. efficiency
19°	73.1%	95.2%
22°	78.1%	95.4%
25°	78.2%	95.1%
28°	75.7%	94.6%
31°	73.1%	93.8%

**Table 4.2:** Efficiency values for design 2.

Table 4.3 shows that design 2 outperforms design 1. The maximum efficiency differential between the two is 0.6%. The total average efficiency difference is 1.7%. The maximum average efficiency difference is 0.5%. All in favor of design 2.

GVO angle	$\Delta$ Max. efficiency
19°	1%
22°	0.7%
25°	0.3%
28°	0.1%
31°	0.7%

**Table 4.3:** Efficiency differentials (design 2 - design 1) for the two designs.

To further showcase the efficiency difference between the designs, the plot viewed in Figure 4.3 shows the different GVO angles at BEP. Efficiencies were also plotted against power output for every GVO angle. Equation 2.7 was used to calculate the power output.

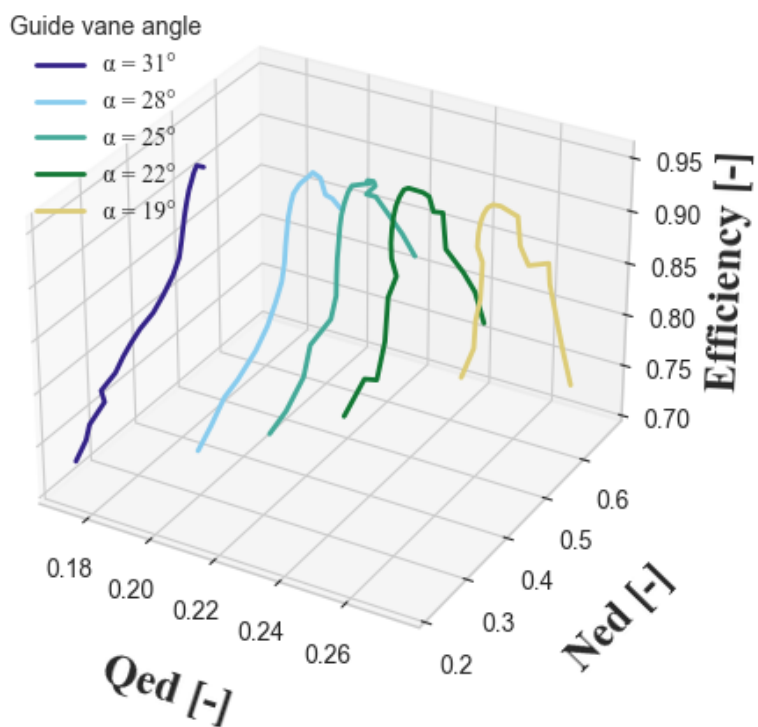
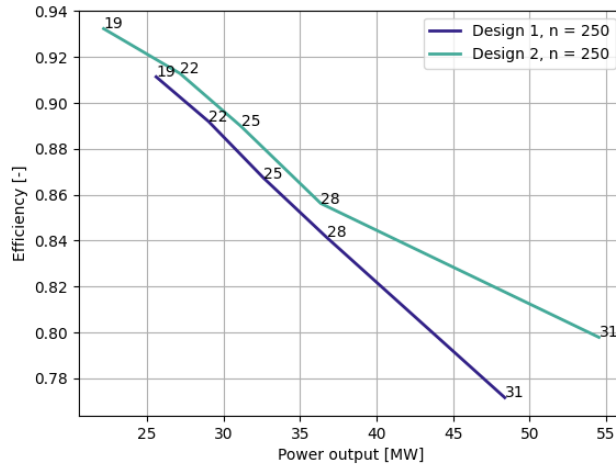
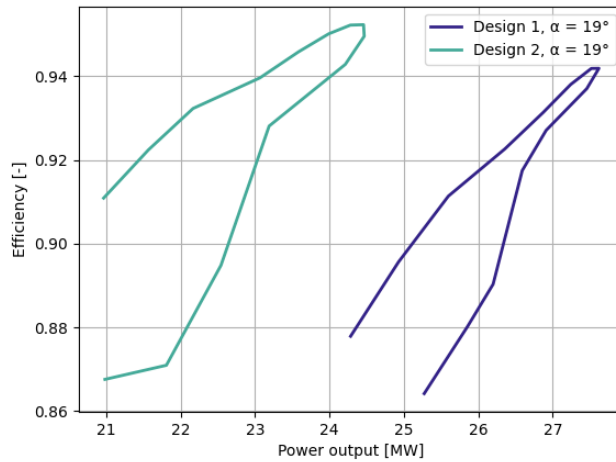


Figure 4.2:  $Q_{ED}$  -  $N_{ED}$  - Efficiency plot for design 2.



**Figure 4.3:** Efficiency plotted against power output for all GVO angles at BEP. Numbers indicate GVO angle.



**Figure 4.4:** Efficiency plotted against power output for a GVO angle of 19°.

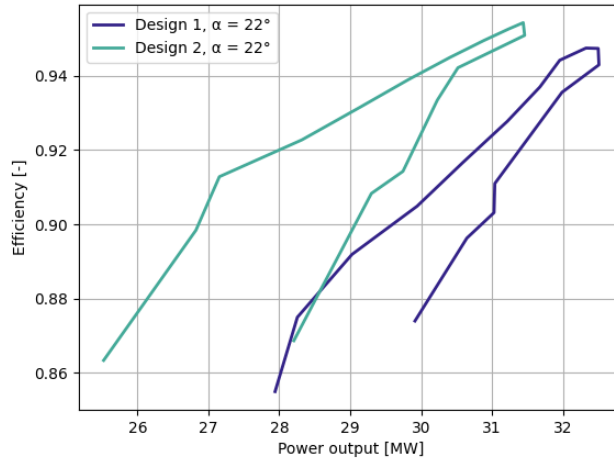


**Figure 4.5:** Efficiency plotted against power output for a GVO angle of  $22^\circ$ .

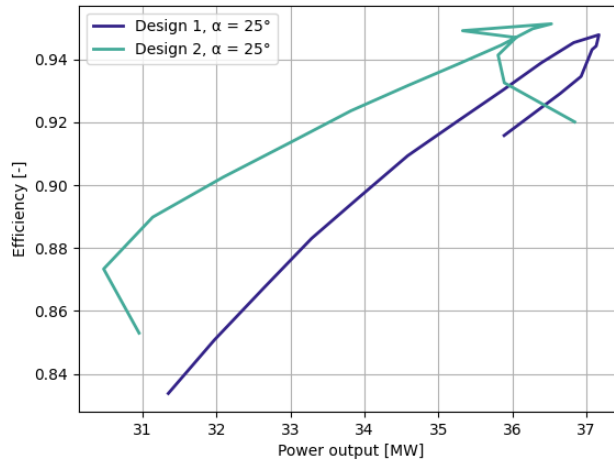


**Figure 4.6:** Efficiency plotted against power output for a GVO angle of  $25^\circ$ .

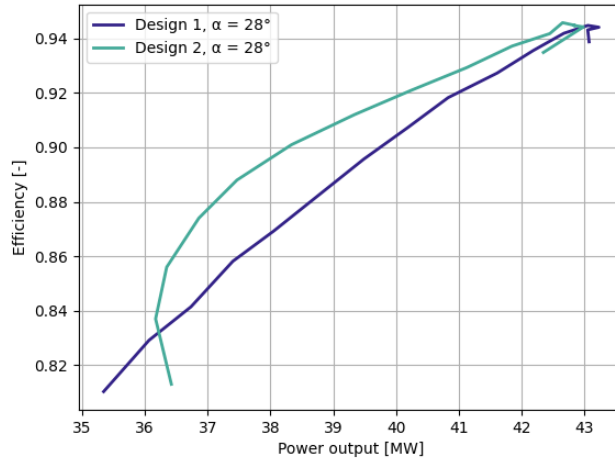


**Figure 4.7:** Efficiency plotted against power output for a GVO angle of  $28^\circ$ .

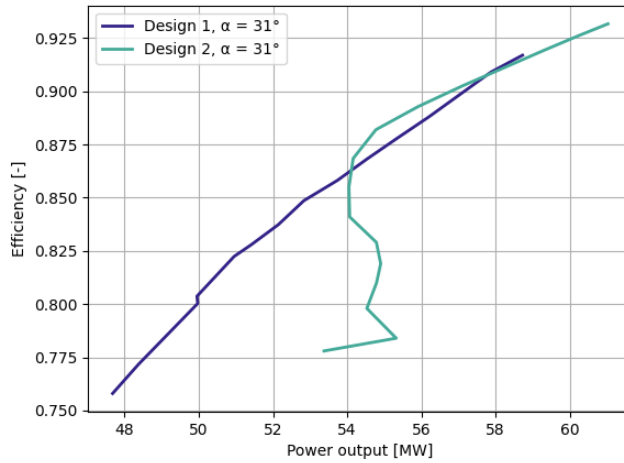


**Figure 4.8:** Efficiency plotted against power output for a GVO angle of  $31^\circ$ .





---

## Chapter V

---

### *Discussion*

The simulation results confirm the hypothesis that the theoretical implementation of a BP will enhance the efficiency in turbine mode for an RPT. The efficiency differentials show meaningful numbers. Hydropower plants can operate for many decades, therefore a 0.5% difference will be quite substantial in the long run. The Roskrepp power plant has a synchronous generator, so varying  $N_{ED}$  values are not majorly relevant. However, from the plots and the data, design 2 operates better at every point for the designed BEP rotational speed as seen in Figure 4.3.

It was originally planned to look at the annual operation for Roskrepp power plant to compare how these designs would perform when operated in the same manner as Roskrepp. However, seeing as design 2 outperformed design 1 everywhere, it was assumed to be obsolete. Therefore, comparing max average efficiencies and max efficiencies for the two machines was considered more than adequate.

Even though the results are quite promising. There are several factors that need to be discussed regarding choices related to the design method and the simulation setup.

Design 2 was created by assuming a 20 meter head difference in pump mode due to the BPs contribution. This thesis has not taken into consideration of how the BP may affect the system. Also, it is uncertain how much extra head the BP will actually produce.

Designing the geometry with Khoj is quite constrained. The input parameters are heavily limited compared to other design tools. Even though Francis turbines and RPTs are quite similar, designing an RPT with Khoj is not the most optimal choice. There are also limitations on the design freedom for the runner blades. The draft tube is also automatically produced, and this component can have a large influence on the efficiency of the machine. The input choices for the guide vanes are also

restricted.

The simulation setups were also not perfect. The accuracy of the results will have deficiencies due to the following reasons: The simulation type was steady state. The flow through an RPT is quite complex and steady state simulations will not be a perfect representation of real life flow. Therefore, transient simulations would be preferred. Rotational periodicity was also used to save computational time and resources. This will also have an impact on the accuracy of the results.

---

## Chapter VI

---

### *Conclusion*

The objective of this thesis was to run simulations on two RPTs. These RPTs were designed with Roskrepp power plant's parameters. The main difference between the designs was the geometrical variations due to the implementation of a BP. It was assumed that the BP contributes with 20 m head in pumping mode.

First, geometry for the designs were produced with the MatLab GUI software Khoj. The geometry files produced in Khoj were exported into ANSYS. Meshes for the designs were created in ANSYS TurboGrid. Steady state CFD simulations were run for one passage in ANSYS CFX. Rotational speeds varying from 200-410 rpm and GVO angles of  $\pm 3^\circ$  and  $\pm 6^\circ$  were simulated for. Rotational periodicity was applied to copy the results around the whole machine. Output parameters to calculate the efficiency were found in CFX Post.

The results from ANSYS found a maximum efficiency difference of 0.6% and a total average efficiency difference of 1.7%. The maximum average efficiency difference was 0.5%. Even though the numerical setup and design method had imperfections. The main goal of the thesis was achieved. Which was to quantify the efficiency difference between two RPTs in generating mode. The results show quite a substantial difference in efficiency between the two designs.



---

## Chapter VII

---

### *Further work*

There are several aspects that could be improved upon in the future. As retrofitting RPTs is completely new there is much research that could be done within this subject, with and without BPs.

A main point for CFD simulations are verifying and validating the results to ensure that they can be trusted. Verification with more thorough CFD simulations would be beneficial. Transient simulations with a full RPT model would be preferred. Also, experimental studies should be performed to be able to validate the results from the simulations.

The diameters were not kept constant with the Roskrepp power plant. A main point of the ongoing study to utilize a BP is the fact that it would potentially not require excavating the turbine space. Therefore, performing a study where the diameters were kept constant would be interesting.

Even though Roskrepp would mainly be operated in turbine mode it would be worthwhile to simulate for pump mode to find the round-trip efficiency. This technology could be used elsewhere where pumping has a larger role, so it would be worthwhile to see if this potential solution is still applicable for such cases. The solution of utilizing a BP in combination with an RPT could be used everywhere that is fitting. Therefore, the potential benefit of this research may be huge if future research validates the results. One disclaimer to this is the fact that the economical aspect has not been investigated.



---

## *References*

- [1] “Renewable energy generation,” URL: <https://ourworldindata.org/grapher/modern-renewable-energy-consumption>.
- [2] “Roskrepp Power Plant,” URL: <https://www.sirakvina.no/roskrepp-kraftverk/roskrepp-kraftverk-article257-921.html>.
- [3] Pacot, O., 2014, “Large Scale Computation of the Rotating Stall in a Pump-Turbine using an Overset Finite Element Large Eddy Simulation Numerical Code,” Doctoral thesis, École Polytechnique Fédérale de Lausanne.
- [4] Nielsen, T. K., 2015, “Simulation model for Francis and Reversible Pump Turbines,” .
- [5] Eltvik, M., “Sediment erosion in Francis turbines,” Doctoral thesis, NTNU Department of Energy and Process Engineering.
- [6] Escher, J. K. L., Dagsvik, H. N., and Storli, P. T. S., 2020, “Design of a reversible pump turbine,” NTNU, Waterpower Laboratory.
- [7] “Skewness of Mesh Structures in ANSYS Meshing,” URL: <https://mechanicalbase.com/skewness-of-mesh-structures-in-ansys-meshing/>.
- [8] “Goal 13: Take urgent action to combat climate change and its impacts,” URL: <https://www.un.org/sustainabledevelopment/climate-change/>.
- [9] J. Hadjipaschalis, V. E., A. Poullikkas, 2008, “Overview of current and future energy storage technologies for electric power applications,” Renewable and Sustainable Energy Reviews.



- 
- [10] L. Lia, K. E. S. G. H. M., T. Jensen and Ruud, A. M., 2015, “The current status of hydropower development and dam construction in Norway,” *Hydropower Dams*.
- [11] Dixon, S. L. and Hall, C. A., 2014, *Fluid mechanics and Thermodynamics of Turbomachinery*, 7th ed.
- [12] Brekke, H., 2000, “Grunnkurs i hydrauliske Strømningsmaskiner,” NTNU, Waterpower Laboratory.
- [13] Brekke, H., 2015, “Hydraulic Turbines: Design, Erection and Operation,” NTNU, Waterpower Laboratory.
- [14] Reines, A. F., 2020, “Analysis and improvement of a mathematical turbine model,” Master thesis, NTNU, Waterpower Laboratory.
- [15] Veersted, H. K. and Malalasekera, W., 2007, *An Introduction to Computational Fluid Dynamics*, 2nd ed.
- [16] Roache, P. J., 1997, “Quantification of Uncertainty in Computational Fluid Dynamics,” .
- [17] Maharjan, N., Chitrakar, S., and Koirala, R., 2014, “Design of Reversible Pump Turbine for its prospective application in Nepal,” .
- [18] Gülich, J. F., 2010, *Centrifugal Pumps*, 2nd ed.
- [19] S. Lazarkiewicz, D. K. R. and Troskolanski, A., 1965, “Impeller pumps,” .
- [20] Stepanoff, A. J., 1957, *Centrifugal and Axial Flow Pumps: Theory, Design, and Applications*, 2nd ed.
- [21] Gjørseter, K., 2011, “Hydraulic Design of Francis Turbine Exposed to Sediment Erosion,” Master thesis, NTNU, Waterpower Laboratory.
- [22] Dahl, G. A., 2014, “Hydraulic design of a Francis turbine that will be influenced by sediment erosion,” Master thesis, NTNU, Waterpower Laboratory.
- [23] Sundfør, E. H., 2017, “Design and operation of a Francis Turbine with Variable Speed Capabilities,” Master thesis, NTNU, Waterpower Laboratory.
- [24] Siggeirsson, E. M. V. and Gunnarsson, S., 2015, “Conceptual design tool for radial turbines,” Master thesis, Chalmers University of Technology, Department of Applied Mechanics.
- [25] ANSYS, 2020, “ANSYS TurboGrid User’s Guide,” .

- 
- [26] ANSYS, 2019, “ANSYS CFX Rotating Machinery Modeling,” .
- [27] Autodesk, 2021, “Autodesk Learning Guide, Turbulent Flow,” .
- [28] Menter, F. R., 1992, “Improved Two-Equation  $k-\omega$  Turbulence Models for Aerodynamic Flows,” NASA, Ames Research Center, California.
- [29] Moritz, R. A. C., 2014, “Transient CFD-analysis of a high head Francis turbine,” Master thesis, NTNU, Waterpower Laboratory.
- [30] C. Trivedi, B. K. G., M. J. Cervantes and Dalhaug, O. G., 2013, “Experimental and numerical studies for a high head Francis turbine at several operating points,” Journal of fluid engineering, vol. 15.
- [31] “Establishing Grid Convergence, URL: <https://curiosityfluids.com/2016/09/09/establishing-grid-convergence/>,” .



---

## Appendix - A

---

### *Gülich Design Method*

This appendix presents impeller calculations for radial pumps from Gülich's book Centrifugal pumps. Here, 1 and 2 denotes turbine inlet and outlet respectively.  $c$  are the absolute velocities.  $w$  is the relative velocity.

$Q$ ,  $H$  and  $n$  are known parameters taken from the Roskrepp power plant. Everything is designed with the BEP in mind. The fluid flow into the pump impeller is mostly axial ( $\alpha_2 = 90^\circ$ ). This means that there is no swirl, so the circumferential component of the absolute inflow velocity is  $c_{u2} = 0$ .

$15^\circ < \beta_1 < 45^\circ$  Radial impellers with 5 to 7 blades are commonly in this range. Usually somewhere between  $20^\circ$  and  $27^\circ$ . Matching angle and outlet width is an optimization process. This process has to be considered with efficiency and stability of the Q-H curve. [18]

To find the circumferential speed:

$$u_2 = \pi D_2 \frac{n}{60} \quad (\text{A.1})$$

Relative velocity:

$$w_2 = \sqrt{c_{m2}^2 + (u_2 - c_{u2})^2} \quad (\text{A.2})$$

Flow angle:

$$\beta_2 = \arctan \frac{c_{m2}}{u_2 - c_{u2}} \quad (\text{A.3})$$

Then the blockage caused by the hub is calculated with the following equation:

$$k_n = 1 - \frac{D_n^2}{D_2^2} \quad (\text{A.4})$$

Where  $D_n$  is the hub diameter. The hub diameter is given by mechanical design optimization. At the outlet, it should be selected close to minimum,  $v_{2,min} \approx 0.15$  (See Equation A.5). At the inlet, it should match the impeller hub. A large hub diameter helps to increase the head developed by centrifugal forces. [18]

$$v_{2,min} = \frac{D_n}{D_2} \quad (\text{A.5})$$

Then, the outlet diameter can be found with the following equation:

$$D_2 = 2.9 \times \sqrt[3]{\frac{Q}{nk_n \tan \beta_2} \left(1 + \frac{\tan \beta_2}{\tan \alpha_2}\right)} \quad (\text{A.6})$$

Since  $\alpha_2 = 90^\circ$ , Equation A.6 will simplify to:

$$D_2 = 2.9 \times \sqrt[3]{\frac{Q}{nk_n \tan \beta_2}} \quad (\text{A.7})$$

---

## Appendix - B

---

### *Uncertainty Analysis*

Uncertainty analysis was performed on three chosen key parameters. The parameters are torque, head and efficiency. This was done to ensure these points converged and provided stable results. The uncertainty analysis was done for the BEP for both designs. This point has 250 rpm and a GVO angle of 25°. The simulations were run for 400 iterations. The values are taken at iteration 300, 350 and 400. The value with the largest discrepancy will be used as a baseline for the uncertainty.

The numbers indicate what the value was at the given iteration.

#### **Design 1:**

<b>Parameter</b>	<b>300</b>	<b>350</b>	<b>400</b>	<b>Uncertainty</b>	<b>%</b>
Head [m]	91.552	91.572	91.556	0.02	0.021%
Torque [J]	-2.168+5	-2.1673E+5	-2.1667E+5	130	0.059%
Efficiency	0.86757	0.867	0.8666	0.00097	0.112%

**Table B.1:** Uncertainty analysis results for design 1.

#### **Design 2:**

<b>Parameter</b>	<b>300</b>	<b>350</b>	<b>400</b>	<b>Uncertainty</b>	<b>%</b>
Head [m]	76.919	76.949	76.9	0.049	0.061%
Torque [J]	-2.6454E+5	-2.6457E+5	-2.6456E+5	30	0.011%
Efficiency	0.88926	0.88921	0.88928	0.0007	0.008%

**Table B.2:** Uncertainty analysis results for design 2.

As can be seen from the tables, the uncertainties are well below 1% and are therefore deemed acceptable for the simulations.

---

## Appendix - C

---

### *Grid Convergence Index*

To further verify that the meshes produced were at an acceptable level, a grid convergence study was performed. This process and the results from this test will be provided here. [31]

A summary of the steps taken:

1. Perform at least three simulations with varying levels of mesh quality.
2. Choose parameter(s) indicative of convergence. In general, this should be parameters that are important for the results of the simulation.
3. Calculate order of convergence.
4. Calculate grid convergence index for the different refinement levels.
5. Ensure that the grids are in asymptotic range of convergence.

For this thesis, five mesh qualities were simulated for. The monitor parameters chosen were the efficiency, torque and pressure difference at inlet and outlet.

The order of convergence,  $p$ , is calculated with the following equation: [31]

$$p = \ln \frac{(f3 - f2)}{\frac{(f2 - f1)}{\ln(r)}} \quad (\text{C.1})$$

Where  $r$  is the ratio of refinement between the mesh sizes.  $f1$  to  $f3$  are the results from every mesh quality level. [31]



Then, the grid convergence index is calculated to identify the convergence quality. It is calculated for the differing mesh qualities. It is defined as such:

$$GCI = \frac{F_s |e|}{r^P - 1} \quad (\text{C.2})$$

Here,  $e$  is the error between the grids.  $F_s$  is an optional, but recommended safety factor. It is chosen as 1.25. [31] These grid convergence indices are calculated for the different monitor points.

To ensure grid deviations are within acceptable levels, it is necessary to check if they are inside the asymptotic range of convergence. If the results show that this is not true, then the solution is not mesh independent. With a minimum of three grids, it can be calculated with the following equation:

$$\frac{GCI_{2,3}}{r^P \times GCI_{1,2}} \approx 1 \quad (\text{C.3})$$

In Table C.1, 1 and 2 denotes design 1 and design 2 respectively. This was done for the three finest meshes. The results following these steps are provided in the table below:

<b>Parameter</b>	<b>p</b>	$GCI_{2,3}$	$GCI_{1,2}$	$\approx \mathbf{1}$
Pressure 2	-1.27	0.5%	0.6%	1.0012
Pressure 1	4.44	0.2%	0.1%	1.0009
Torque 2	-2.43	0.1%	0.1%	1.0004
Torque 1	0.65	0.6%	0.5%	1.0006
Efficiency 2	-1.07	0.4%	0.5%	1.0008
Efficiency 1	-2.57	0.3%	0.5%	1.0016

**Table C.1:** Grid Convergence Index results.

As seen in Table C.1, for all monitor points, the values are within the asymptotic range. Therefore, it can be concluded that the meshes are acceptable. The deviations are not too large from the finer meshes and mesh independence has been achieved.

